Climate Dynamics (2002) 19: 123–140
DOI 10.1007/s00382-001-0218-4

V.A. Semenov · L. Bengtsson

Secular trends in daily precipitation characteristics: greenhouse gas simulation with a coupled AOGCM

Received: 27 February 2001 / Accepted: 28 November 2001 / Published online: 26 April 2002

Abstract Secular trends of daily precipitation characteristics are considered in the transient climate change experiment with a coupled atmosphere–ocean general circulation model ECHAM4/OPYC3 for 1900–2099. The climate forcing is due to increasing concentrations of the greenhouse gases in the atmosphere. Mean daily precipitation, precipitation intensity, probability of wet days and parameters of the gamma distribution are analyzed. Particular attention is paid to the changes of heavy precipitation. Analysis of the annual mean precipitation trends for 1900–1999 revealed general agreement with observations with significant positive trends in mean precipitation over continental areas. In the 2000–2099 period precipitation trend patterns followed the tendency obtained for 1900–1999 but with significantly increased magnitudes. Unlike the annual mean precipitation trends for which negative values were found for some continental areas, the mean precipitation intensity and scale parameter of the fitted gamma distribution increased over all land territories. Negative trends in the number of wet days were found over most of the land areas except high latitudes in the Northern Hemisphere. The shape parameter of the gamma distribution in general revealed a slight negative trend in the areas of the precipitation increase. Investigation of daily precipitation revealed an unproportional increase of heavy precipitation events for the land areas including local maxima in Europe and the eastern United States.

V.A. Semenov (✉) · L. Bengtsson
Max-Planck-Institut für Meteorologie,
Bundesstrasse 55, 20146 Hamburg, Germany
E-mail: semenov@dkrz.de

Permanent affiliation: V.A. Semenov
Obukhov Institute of Atmospheric Physics,
Russian Academy of Sciences, Pyzhevskiy 3,
109017 Moscow, Russia

1 Introduction

Trends in mean precipitation for the twentieth century have been documented in a number of studies based on global and regional observational data (Bradley et al. 1987; Diaz et al. 1989; Dai et al. 1997; Vinnikov et al. 1990; Karl et al. 1996; Groisman and Easterling 1994). For the globe a 1–2% secular upward trend was found for the land precipitation in twentieth century. A significant positive trend was observed in high and mid latitudes in the Northern Hemisphere (NH, more pronounced in the second half of the century) with concurrent decrease in low-latitude precipitation (Bradley et al. 1987; Diaz et al. 1989; Dai et al. 1997). In the Southern Hemisphere (SH) precipitation over land areas had a positive trend for all latitudes (Diaz et al. 1989), although the data quality leaves a wide range of uncertainty. Studies focused on the continental and regional scale support the overall picture of the precipitation changes. So, for example, an annual precipitation increase was recorded during the last century or last 50 years in the contiguous United States and Canada (Groisman and Easterling 1994; Karl and Knight 1998), northern Eurasia (Wang and Cho 1997), former Soviet Union (Vinnikov et al. 1990), Australia (Suppiah and Hennessy 1998) and South America (Diaz et al. 1989).

An important question is how the precipitation trends may be projected in the future as a consequence of global warming. Calculations from coupled atmosphere–ocean general circulation models (AOGCM) reveal in general consistent precipitation change patterns in response to a doubling of the CO_2 concentration in the atmosphere. Most AOGCMs are in broad agreement in producing more precipitation in high latitudes and in the tropics throughout the year and in the mid-latitudes in winter (Houghton et al. 1996). In the transient climate change experiment with ECHAM4/OPYC3 AOGCM investigated here (an experiment with increasing concentration of greenhouse gases in the atmosphere

described by Roeckner et al. 1999, hereafter referred to as GHG), global precipitation over land started to rise rapidly from about the 1950s and increased by about 11% at 2100. The precipitation increase over the oceans is only 0.1%. Significant precipitation changes are caused by a strong warming at high latitudes in both hemispheres during cold seasons, by an intensification of the ITCZs around the globe, by stronger monsoon circulation with an associated increase in the monsoon precipitation, and finally as an enhancement of precipitation in the extratropical storm tracks. A tendency of reduced precipitation is found in some tropical and subtropical ocean regions, some coastal parts of the continents and around the Mediterranean Sea.

A very important issue for social and economical impacts of the forthcoming changes in the hydrological cycle is the short-term precipitation variability such as extreme events in the form of heavy rains or snowfalls associated with possible change in the statistical properties of precipitation. A warming due to the greenhouse gas forcing leads to exponential growth (according to the Clausius-Clapeyron equation) of the water-holding capacity of the atmosphere. With a little change in relative humidity this means an (about exponentially) increased moisture content in the atmosphere. These considerations are supported by coupled AOGCM climate change simulations which produce more than 20% increase in the atmospheric moisture due to the warming caused by the CO_2 doubling (Trenberth 1998). The increased moisture content may favour more intense precipitation. However, precipitation changes on a large scale are restricted by the change in evaporation and on smaller scale by changes of the water residence time in the atmosphere. The latter is dependent on the atmospheric dynamics and a specific evaluation of climate change experiments is required to get more robust qualitative results.

The empirical analysis of the extreme precipitation changes or changes in the precipitation distribution is restricted by the lack of long-term daily precipitation time series. Recent development of station precipitation datasets comprising century long daily precipitation data for different areas (Karl et al. 1996; Karl and Knight 1998; Suppiah and Hennessy 1998; Gruza et al. 1999; Zhai et al. 1999), made it possible to estimate a long-term variability of the daily precipitation characteristics. Significant increases in heavy precipitation were found for the United States, the European part of the FSU and eastern Australia.

Despite availability of the daily precipitation data from GCM experiments only a limited number of studies of the daily precipitation statistics changes caused by global warming have been performed (Gregory and Mitchell 1995; Hennessy et al. 1997; Zwiers and Kharin 1998; McGuffie et al. 1999; Kharin and Zwiers 2000; Voss et al. 2002). In these studies an increase of the heavy precipitation at the expense of the light precipitation events was found for many land areas including Europe.

Of particular interest are transient climate change experiments which allow an examination of the long-term variations. In this study results of the GHG climate change experiment with the coupled ECHAM4/OPYC3 AOGCM are analyzed for the period of 1900–2099. Daily precipitation statistics are described by parameters of a simple statistical model based on the gamma distribution. The use of a theoretical distribution instead of quantiles, return periods and other indices of the precipitation statistics derived directly from the daily data gives a loss of some accuracy due to the impossibility of the chosen distribution function adequately describing precipitation statistics all over the globe. However, an analysis of the fitted distribution parameters allows one to evaluate the changes of the entire range of precipitation distribution on the global scale and helps to understand physical mechanisms of the formation of the distribution and its change.

The study is organized as follows: in Sect. 2 the data used are described, and Sect. 3 is devoted to the validation of the model ability to simulate global mean precipitation structure and trends in the twentieth century as well as an index of heavy precipitation. In Sect. 4 the gamma distribution model applied to describe statistical properties of the daily precipitation is discussed. The parameters of the statistical model for the present climate (1961–1990) are shown in Sect. 5. In Sect. 6 twenty first century trends of the analyzed daily precipitation parameters are presented and in Sect. 7 area-averaged precipitation characteristics are shown for Europe and United States. In Sect. 8 the results obtained are discussed.

2 Data used

Global daily precipitation data from a numerical experiment with the AOGCM ECHAM4/OPYC3 (Oberhuber 1993; Roeckner et al. 1996a) were used for the analysis. The atmospheric model has a T42 spectral horizontal resolution (approximately 2.8° latitude/longitude). In this experiment (Roeckner et al. 1999) greenhouse gas (GHG) concentrations in the atmosphere for 1860–1990 were taken according to observations and for 1991–2100 according to IS92a "business as usual" scenario (Houghton et al. 1992) describing GHG growth due to expected human population increase and industry development. Following this scenario total radiative forcing due to GHG reached 2.7 W/m^2 in year 2000 and 7.6 W/m^2 in 2100 (relative to the preindustrial time), which corresponds approximately to the doubling and tripling of the equivalent CO_2 concentration in the atmosphere in the middle and at the end of the twenty first century, respectively.

For model validation the global precipitation climatology for 1979–1995 (Xie and Arkin 1997), land precipitation climatology for 1961–1990 (New et al. 1999) and 1901–1996 land precipitation dataset (New et al. 2000) were used. For comparison with the model results these data were interpolated to the model resolution using the model land–sea mask.

3 Twentieth century simulation results: model validation

The atmospheric model performance for the present climate is analyzed in Roeckner et al. (1996a). Climate

variability associated with ENSO in the coupled model was considered by Roeckner et al. (1996b). The simulation of the precipitation in the ECHAM4 model at different resolutions is discussed by Stendel and Roeckner (1998). The general results of the scenario climate change experiments including the experiment analyzed in this study are considered in Roeckner et al. (1999). Analysis and validation of the hydrological cycle on a regional scale were performed in Arpe and Roeckner (1999), Arpe et al. (1999), and Hu et al. (2000). In particular, a comparison of the model precipitation for Europe with different observational analyses showed that the model was able to reproduce the main features of the hydrological cycle within the range of uncertainty of the observational data (Arpe and Roeckner 1999).

In this section we will briefly consider the model's ability to simulate the mean precipitation for the present reference climate (defined as an average for 1961–1990 period). Long-term changes in the annual mean precipitation will be validated by comparison with twentieth century observed precipitation trends over land (New et al. 2000). The ability of the model to capture twentieth century changes in heavy precipitation related to daily precipitation distribution change will be presented using an index derived from observed and simulated daily data for the United States.

3.1 Mean precipitation

Model annual mean global precipitation for the reference climate is compared to the observed data for 1979–1997 from Xie and Arkin (1997) (Fig. 1, using model average for 1979–1997 does not modify the results). Zonal mean values for land and ocean are presented in Fig. 2. For the land areas also a climatology for 1961–1990 (New et al. 1999) is used. As can be seen from Figs. 1 and 2 the model reproduces the mean precipitation pattern reasonably well. The model overestimates annual mean precipitation over continents in general except for northern Africa, India, the north- and southeastern coasts of South America, and an area north of the Gulf of Mexico. In particular, over Europe the overestimation is due to high winter precipitation (with minor overestimation in autumn and spring) while in summer precipitation is underestimated (not shown). Over the ocean the highest discrepancies are found in the tropical belt in the regions with the most intense precipitation. The model produces excessive precipitation in the tropical Indian ocean and in the regions of the ITCZ and SPCZ, with less precipitation east to the Indian and southeastern Asia coasts and in the western equatorial Pacific. It should be noted that the observed data for these regions mostly comprise indirect satellite observations and reanalysis data (Xie and Arkin 1997).

3.2 Precipitation trends

The simulated and observed relative trends of annual mean precipitation over land are presented in Fig. 3a, b respectively. The global land precipitation (excluding Antarctica) absolute trend value for 1901–1996 is 0.073 mm/day (3.5% relative to the reference climate) in the model and 0.050 mm/day (2.6%) in observed data. Although there is a broad agreement between the simulated and observed precipitation trends, there are also regional differences. This is both due to model limitations and to data deficiencies. A significance test carried out on the model result suggests that the most reliable trend occurs at higher latitudes of the Northern Hemisphere. The large differences in the relative trend over Sahara, south Arabia, western Asia and other arid regions may, in particular, be caused by very low precipitation amounts.

3.3 Validation of change in heavy precipitation

To examine the model's ability to simulate the trend in the intense daily precipitation, the contribution of the upper 10% daily precipitation quantile to the total annual amount was averaged for the USA (quantiles were computed for the reference climate). This index was chosen for the comparison as a dimensionless quantity representing changes in heavy precipitation over continental-scale area and it comprises perhaps the most extensive (in time and space) available station dataset. It was compiled by Karl and Knight (1998) based on the long-term (1910–1996) daily precipitation records from about 200 stations across the contiguous United States. As can be seen from Fig. 4 the model reproduced quite well the positive trend, the mean and the amplitude of the interdecadal variability. The magnitude of the trend is 2.7% against 4% in the Karl and Knight (1998) data.

4 Statistical model of daily precipitation

A variety of statistical models describing daily precipitation has been proposed (Woolhiser and Roldan 1982; Stern and Coe 1984; Juras 1994). When trying to describe the distribution of the daily precipitation time series one faces two competing requirements, namely the need to obtain the best fit to the data and to do so with a minimum of parameters that are easy to interpret.

As a compromise between these requirements a gamma distribution has been chosen. Although a number of other distributions such as Weibull, Pearson Type 3, log-normal, Poisson-exponential and others could be used for the same purposes, the choice of the gamma distribution is preferable as it has been widely used in meteorology for describing the distribution of observed and model-generated precipitation (Gregory et al. 1993; Gregory and Mitchell 1995; Wilks 1995; Katz 1999; Groisman et al. 1999). It also provides a good fit to the data. The properties of the gamma distribution and methods of fitting it to the data have been discussed in the literature (Thom 1958; Katz 1977, 1999; Wilks 1990, 1995).

The gamma distribution $g(x)$ provides a flexible family of positively skewed distributions and it is determined by its shape (α) and scale (β) parameters:

$$g(x) = \frac{1}{\beta^{\alpha}\Gamma(\alpha)} x^{\alpha-1} \mathrm{e}^{-x/\beta}, \quad x, \alpha, \beta > 0 \ .$$

where Γ is the gamma function. Depending on its shape parameter α, the gamma distribution may vary from hyperbolically increasing

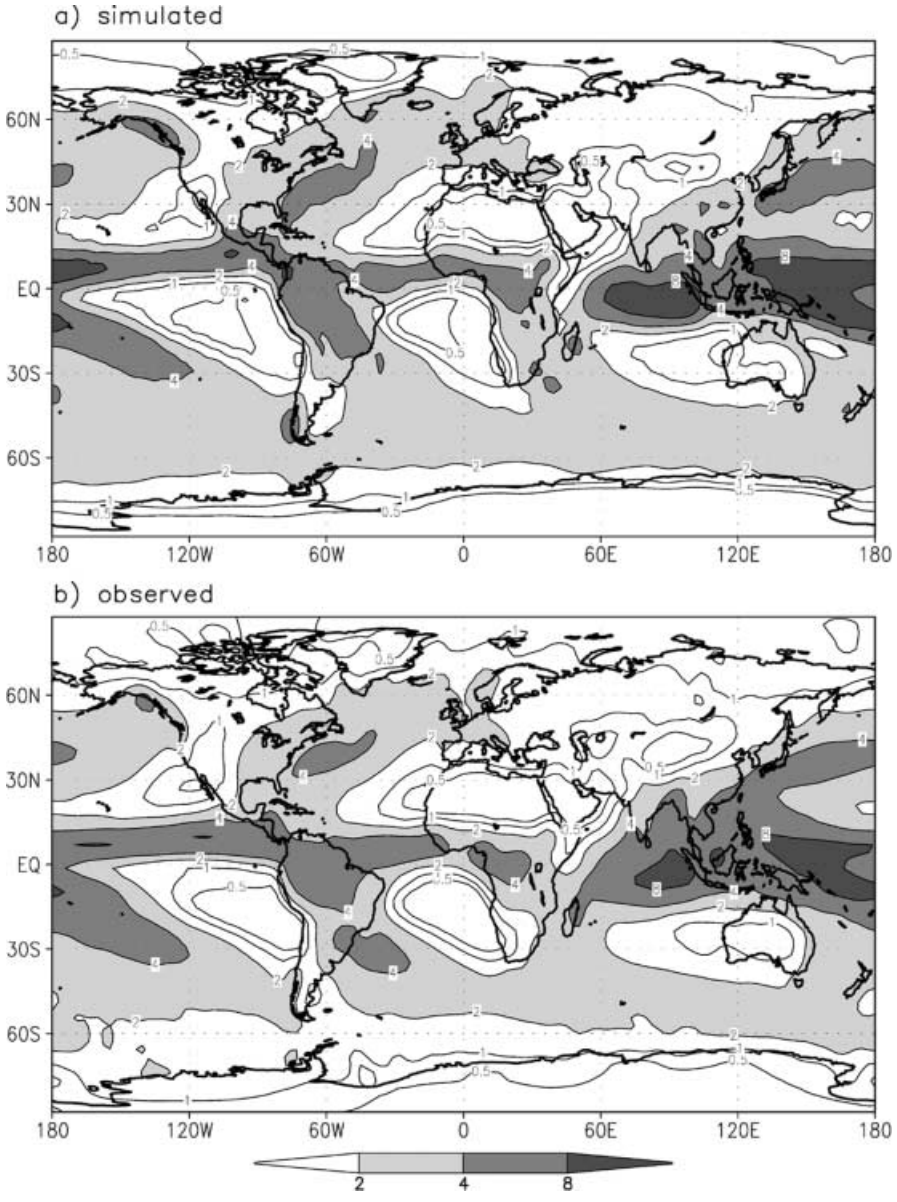

Fig. 1. **a** Annual mean precipitation, mm/day, 1961–1990, model; **b** CMAP analysis, 1979–1997. Values greater than 2 are *shaded*. Contours are at 0.5, 1, 2, 4, 8

when x approaches zero ($\alpha < 1$), becoming an exponential distribution ($\alpha = 1$), or asymptotically approaching a normal distribution when $\alpha \to +\infty$ (see Fig. 5).

As the gamma probability density function describes only the distribution of the non-zero arguments, an unconditional (for both dry and wet days) cumulative distribution function (cdf) of precipitation amounts is given by

$$F(x) = 1 - P_w + P_w G(x) \ ,$$

where x is the precipitation amount, $G(x)$ is the gamma cdf, and P_w the probability of wet days.

Mean precipitation ($\bar{p}$) and mean precipitation intensity (p_I) can now be written as follows:

$$\bar{p} = P_w \alpha\beta \ ,$$

$$p_I = \alpha\beta \ ,$$

Figure 5 illustrates the forms of the gamma distribution corresponding to different values of the parameters α and β. For all three curves the product of the parameters or precipitation intensity (p_I) is equal to 4 mm/day which approximately corresponds to the mean summer precipitation intensity for mid-latitudes of the Northern Hemisphere. It can be clearly seen from Fig. 5b, that for sufficiently large values of daily precipitation (more than 10 mm/day for the present case) the probability density function (pdf) on the logarithmic scale is very well approximated by a straight line with a slope of $1/\beta$. This implies corresponding exponential growth for the probability of the high precipitation rates. This approximation holds when $1/\beta \gg |\alpha - 1|/x$, where x is daily precipitation.

To estimate the parameters of the gamma distribution a method of maximum likelihood is most efficient (in comparison to the methods of conventional and probability-weighted moments). In meteorological application this method in comparison with conventional moments estimators was discussed by Thom (1958), who derived simple approximations of the likelihood solutions. In our study a precise solution of the likelihood equations (Wilks 1995) was used. It should be noted that use of the L-moments method (Hoskins 1990) gives very similar results and is competitively efficient for large samples (> 100) with the advantage of much less computation.

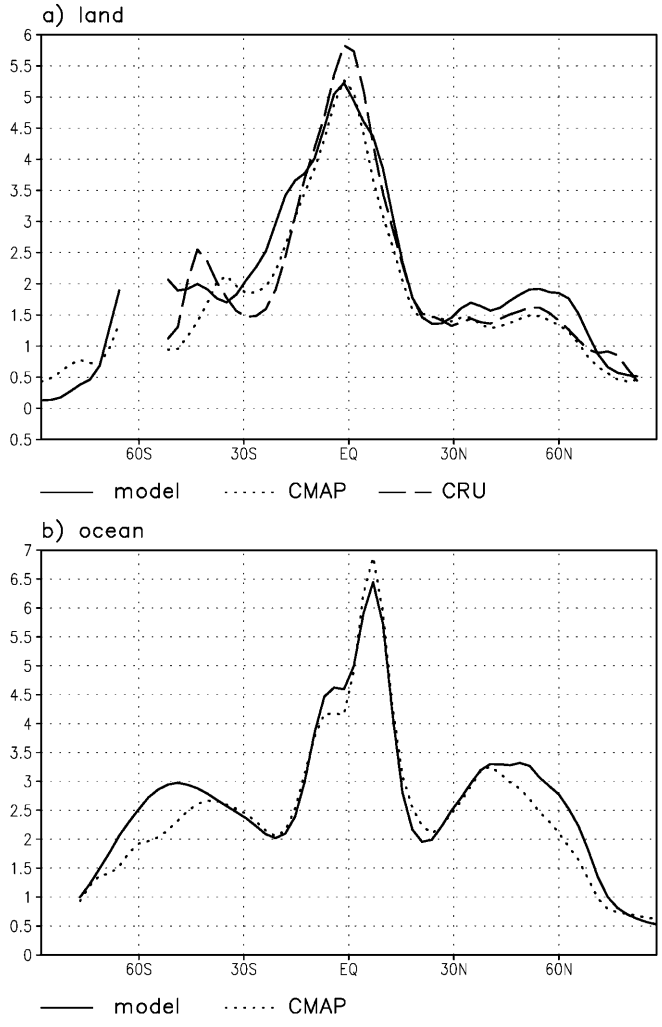

Fig. 2. Zonal mean values of the annual mean precipitation for **a** land and **b** ocean. *Thin line*, simulated, 1961–1990; *dotted line*, observed Xie and Arkin (1997); *dashed*, observed New et al. (1999), mm/day

Very small daily precipitation amounts may be caused by numerical noise and truncation errors in data archiving procedures in atmospheric models and therefore a precipitation threshold is usually used to determine a "wet" day. We used $P_0 = 0.1$ mm/day as the threshold thus fitting a gamma distribution to the $\{P_j - P_0\}$, where $\{P_j\}$ are daily precipitation values exceeding P_0. Here the index j spans a number of "wet" days within a particular season.

The parameters of the gamma distribution were estimated for different seasons for every year for 1900–2100 assuming quasi-stationarity of the precipitation time series on the seasonal timescale.

To estimate the accuracy of the gamma distribution model non-parametric goodness-of-fit, the Kolmogorov-Smirnov test based on the empirical distribution function (D'Agostino and Stephens 1986) was applied for every season for 1900–2099. The results presenting the number of model cells (in percent) where the null-hypothesis that the data sample is drawn from the gamma distribution is rejected at the 10% confidence level are shown in Table 1 for land and ocean separately. As can be seen from the Table 1 the fit of the gamma distribution is much better for the land areas, with less than 5% of the model cells where the null-hypothesis is significantly rejected. For the ocean the fit is worse and varies in the mean from 11.9% for September, October, November (SON) to 17.5% for December, January, February (DJF). Areas of frequent rejection are normally associated with small values of the shape parameter (usually lower than 0.6). The fit is much worse if the daily data for the entire year are taken (Table 1).

5 Precipitation characteristics for the present climate

The parameters of the gamma distribution were calculated for every season of 1900–2099. In this section the mean values of these parameters, wet day probability, precipitation, and precipitation intensity are presented for the reference climate (1961–1990). Parameters of the gamma distribution were not estimated for the model cells with fewer than five days with precipitation per season. These areas are marked as missing values (colored black) in the corresponding figures.

5.1 Precipitation intensity and wet day probability

In Fig. 6 JJA and DJF seasonal mean patterns of precipitation, precipitation intensity and wet day probability are presented. As can be seen, the main differences between JJA and DJF patterns are due to seasonal variations of the storm track precipitation in the North Pacific and North Atlantic oceans, monsoon precipitation (particularly distinguished over India and east Asia), ITCZs and "warm pool" precipitation. Note that the precipitation intensity pattern does not always follow the mean precipitation. In particular there is no minimum in the precipitation intensity at the western part of the United States due to the low wet day probability. A noticeable difference in precipitation and wet day probability is observed over Southern Hemisphere continents with reduced $\bar{p}$ and P_w during JJA and enhanced during DJF. In particular, P_w may vary by an order of magnitude (from 0.1 to 0.9 for JJA and DJF respectively) in the middle part of South America and in southern Africa.

5.2 Shape and scale parameters

The mean shape and scale parameters of the gamma distribution for JJA and DJF are shown in Figs. 7 and 8. The shape parameter is less than 1 for most land and ocean areas which assumes an over-exponential form of the precipitation distribution. Over the ocean values of the shape parameter exceeding 1 are found in regions with low precipitation in the tropics close to the western coasts of the continents (less pronounced in the Northern Hemisphere during DJF in accordance with the seasonal precipitation pattern, Fig. 6) and in the storm track areas (North Atlantic and Pacific during DJF and along 60°S during JJA). During JJA the shape parameter exceeds 1 over land in the central United States (east of the Rocky Mountains, following the model orography), Mexico and the northern tip of South America, in central Africa

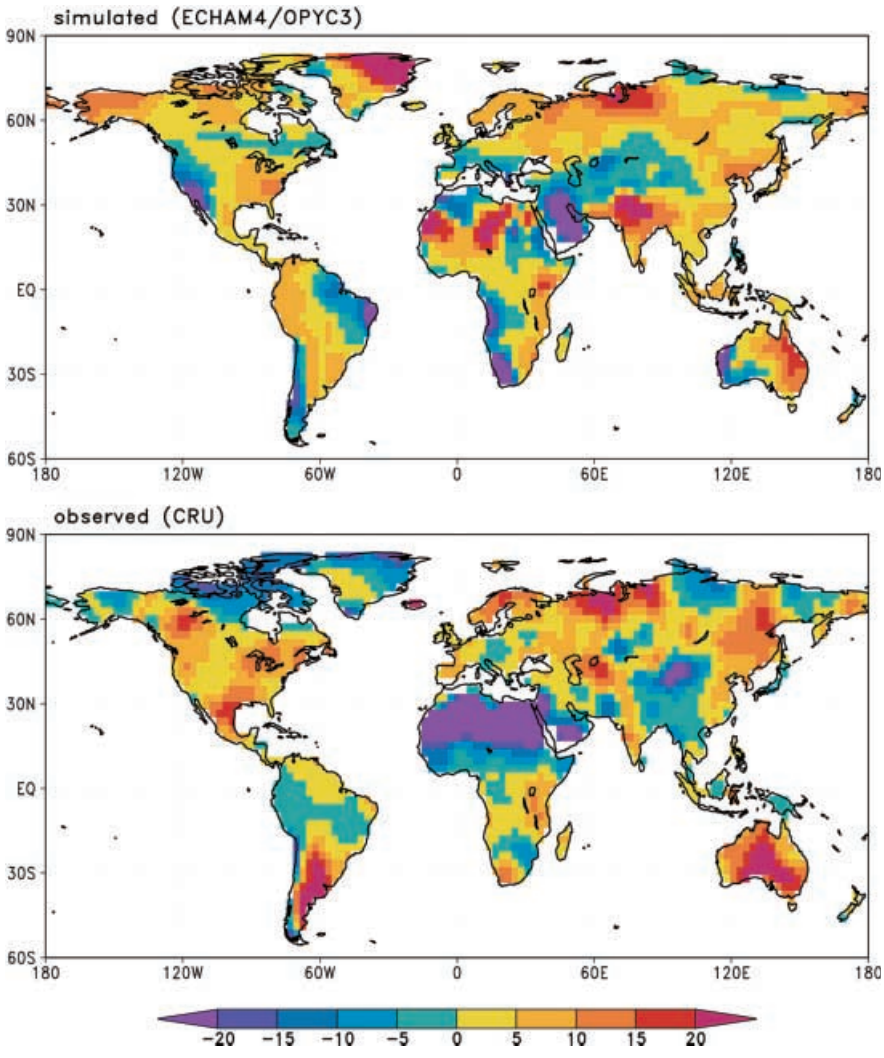

Fig. 3. Precipitation trends (1901–1996), **a** simulated and **b** observed New et al. (2000), %/100 years

north of the Equator, and over the Tibetan Plateau and southern China. For DJF $\alpha > 1$ is found east of the Andes in South America and in continental South Africa. Except for the mentioned areas, the shape parameter over land does not usually exceed 0.8.

The scale parameter in general follows very well the pattern of the precipitation intensity (pattern correlation is more than 0.9). The zonal mean values of the scale parameter vary by a factor of 10 from high latitudes to the equatorial area (from about 1 to 10 mm/day), whereas the features of the zonal distribution of the shape parameter are much weaker and the changes are usually not exceeding 20% of the global land and ocean averages.

Mean seasonal values (for JJA and DJF) of the analyzed precipitation characteristics are summarized in Table 2.

6 Twenty first century trends

Simulated future changes in the precipitation characteristics are described by seasonal (JJA and DJF) linear trends computed for 2000–2099. The trends are represented by a percentage of the mean reference climate (1961–1990) values. The changes in heavy precipitation are illustrated by the index introduced in Sect. 3.

For the gamma distribution parameters the trends were not computed (black areas in the figures) for the model cells where more than 10% of data consisted of missing values (due to insufficient number of wet days for the parameter estimation).

6.1 Mean precipitation

The relative trends in the mean JJA and DJF precipitation for 2000–2099 are presented in Fig. 9a, b respectively. The most pronounced precipitation changes are found in high latitudes of the Northern Hemisphere (north to 50°N) for the winter precipitation which exhibits the strongest upward trends with maximum in northeastern Eurasia reaching 80% (Fig. 9b). During summer the trends are much weaker or even negative for the northern high-latitudes (Fig. 9a). The relative precipitation changes over the ocean in mid- and high-latitudes of the Northern Hemisphere are less intense

but the highest absolute trend values (more than 1 mm/day per century) are found in North Pacific storm track area during DJF and in the North Atlantic close to the Norwegian coast during SON and DJF (not shown).

For the JJA (Fig. 9a), the marked feature is an area of negative trend for the mid-latitudes in Eurasia (30°N–50°N, west to 110°E) with maximum negative trend values (more that 40%) north to the Aral Sea. The negative precipitation trends around the Mediterranean Sea are also found in the other seasons. The opposite signs of the precipitation trends in northern and southern Europe for all seasons except JJA may be related to the intensification of the North Atlantic storm tracks along with an eastward shift of atmospheric centres of action in the model (corresponding to the Icelandic low and Azores high) noticed in this experiment (Ulbrich and Christoph 1999).

A strong negative trend is found in Mexico during DJF and in the western United States and Canada for JJA. In the eastern and high latitudes of North America a positive trend is found for all seasons with a local maximum around the Great Lakes.

The highest positive (relative) trends in the Northern Hemisphere are found in northern India and in arid regions around the Persian Gulf and northern Africa. The positive trend over India is highest in absolute value for the northern continents; is present during all seasons except for DJF and reaches 2 mm/day during JJA.

In the Southern Hemisphere precipitation increases in high latitudes and decreases in mid-latitude ocean areas for all seasons. Over land one can mark strong negative trends in Brazil during JJA (exceeding –80%) and in western Australia (JJA and DJF).

Over the ocean one can see strong positive precipitation trends in the equatorial Pacific and Indian oceans accompanied by negative trends in the adjacent areas. These changes are present for all seasons and maximal in absolute values, exceeding 4 mm/day in the equatorial

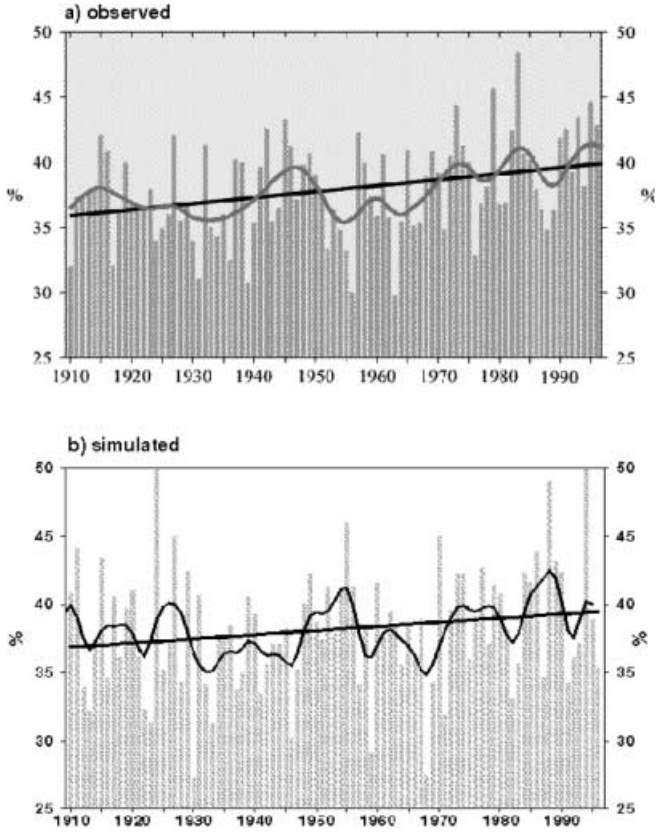

Fig. 4a, b. Contribution of the upper 10% quantile of daily precipitation to the annual total precipitation (area-averaged across USA). **a** Observations, reproduced from Karl and Knight (1998), **b** simulated, ECHAM4/OPYC3 GHG. *Smooth curve* is a nine-point binomial filter

Table 1. A mean (1900–2099) number of the model cells (in %) where the null-hypothesis that a sample originates from the gamma distribution is rejected at the 10% significance level (Kolmogorov–Smirnov statistics)

Season	Land	Ocean
JJA	2.9	17.1
SON	2.5	11.9
DJF	3.6	17.5
MAM	4.2	14.5
Year	18.8	40.2

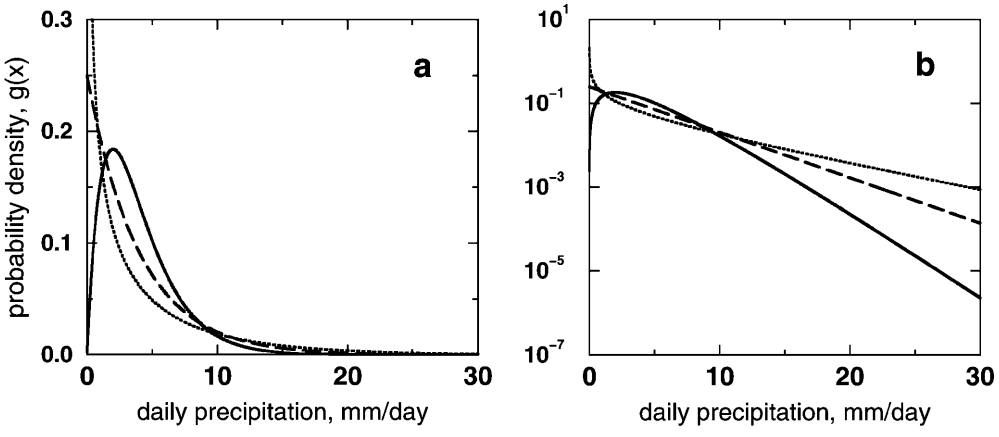

Fig. 5. The gamma distribution probability density function in **a** linear and **b** logarithmic probability axis scales. $\alpha = 2$, $\beta = 2$ mm/day, *solid line*; $\alpha = 1$, $\beta = 4$ mm/day, *dashed line*; $\alpha = 0.5$, $\beta = 8$ mm/day, *dotted line*

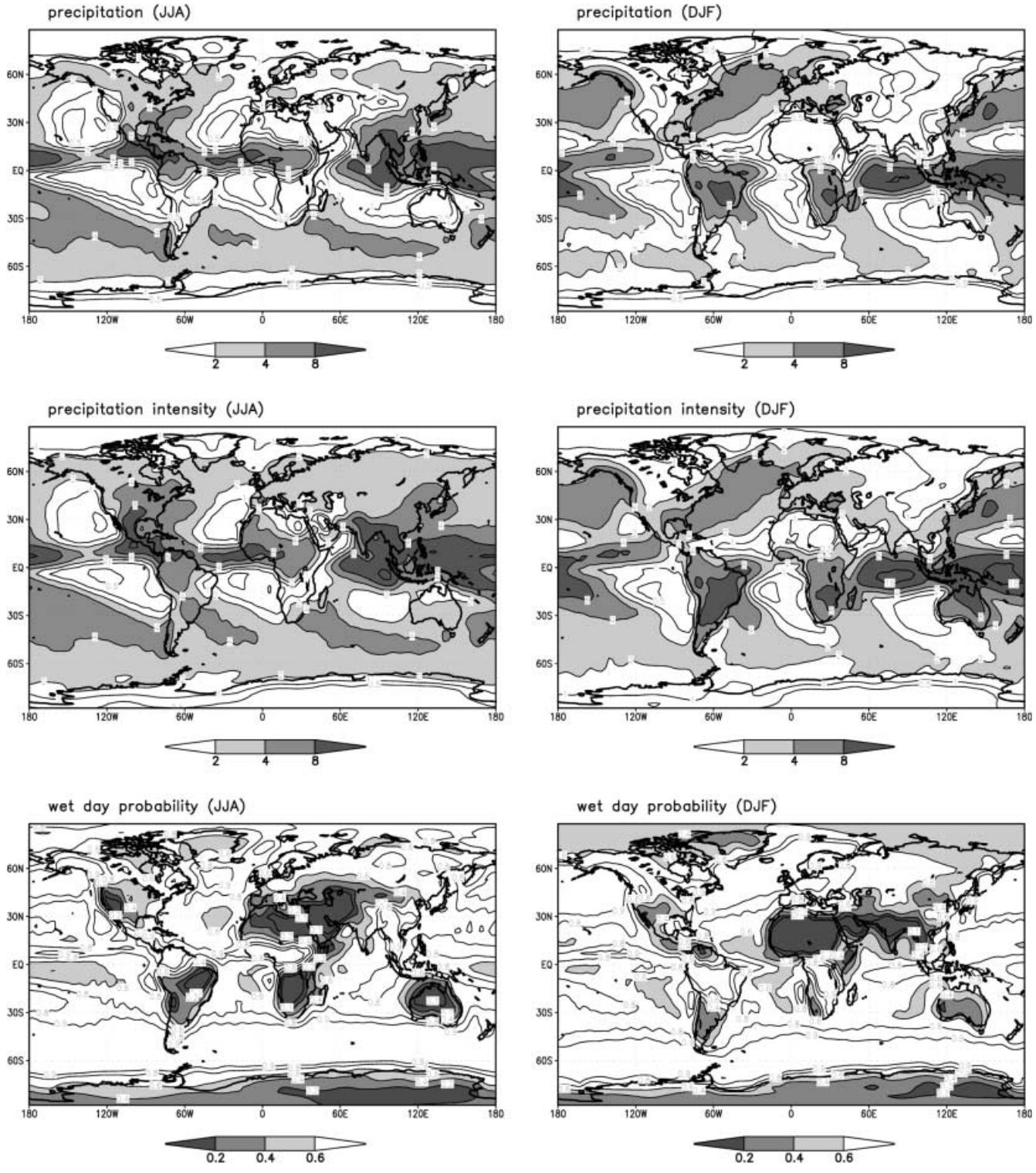

Fig. 6. Seasonal mean JJA (*left column*) and DJF (*right column*) precipitation (mm/day, *upper panels*), precipitaion intensity (mm/day, *middle panels*) and wet day probability (*bottom panels*) simulated for the reference climate. For precipitation and precipitation intensity values greater than 2 are *shaded*, contours are at 0.5, 1, 2, 4, 8, 16. For wet day probability values lower than 0.6 are *shaded*, contours are at 0.1, 0.2, 0.4, 0.6, 0.8, 0.9

belt. This implies not only intensification of the intertropical convergence zones (ITCZs) in the equatorial Pacific and Indian oceans but also a shift in position of the ITCZs.

6.2 Precipitation intensity

The mean precipitation intensity relative trends for JJA and DJF are presented in Figs. 9c, d. It can be seen that

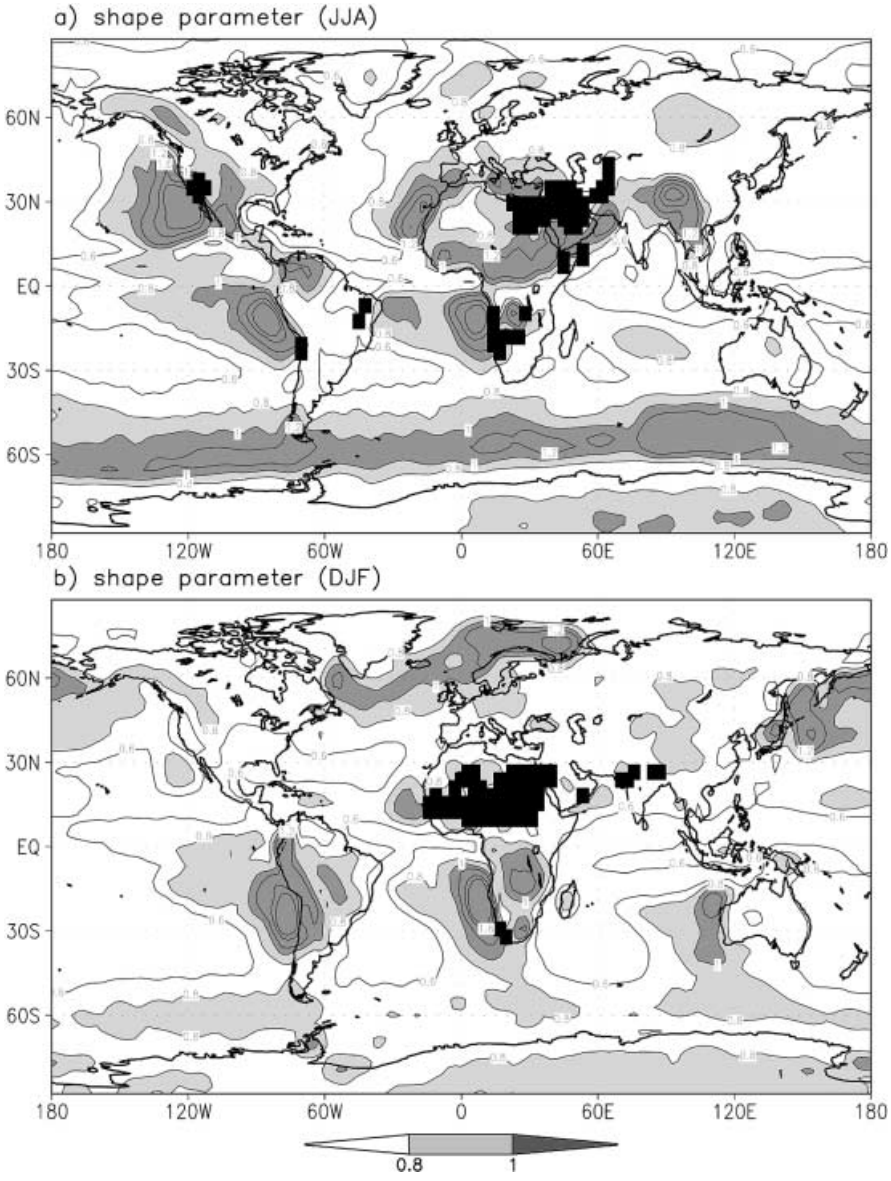

Fig. 7. Shape parameter for **a** JJA and **b** DJF, reference climate. Values greater than 0.8 are *shaded*, contours are at 0.4, 0.6, 0.8, 1, 1.2, 1.6, 2

with the exception of some narrow coastal regions there is a significant positive trend almost for all land areas for JJA and DJF. Noticeable exceptions are northern Africa, India and Mexico during DJF, eastern part of South America, western Australia and an area east to the Caspian Sea during JJA. Note a positive trend over Europe during JJA with maximum exceeding 40% over the Alpine region where only about 5% increase of mean precipitation is found.

6.3 Wet day probability

The difference between the total precipitation and precipitation intensity trends is by definition due to the trends in wet day probability which are depicted in Figs. 9e, f for JJA and DJF respectively. There is a distinguishing zonal structure in the trend pattern in the Northern Hemisphere with a zone of negative trends in mid-latitudes having maximum values around 45°N, which is found for all seasons (less noticeable for DJF). This structure is most pronounced during JJA (Fig. 9e) when most of the global land areas (with noticeable exceptions of India and northeastern Africa) and northern oceans have negative P_w trends. During DJF (Fig. 9f) and transient seasons (not shown) the most marked changes happen in northern high-latitudes as strong increase of wet day probability. Positive century trends exceed 40% for the Arctic that implies more than 0.1 in absolute value. This zonal change is in agreement with the results of the UKHI and CSIRO models' equilibrium climate change experiments (Hennessy et al. 1997). The strongest negative P_w trends in mid-latitudes in Eurasia including local extrema in Central Europe and western United States are related to the mean precipitation decrease in this area described (Fig. 9a) and accompanied by (in general) a moderate increase in precipitation intensity (Fig. 9c).

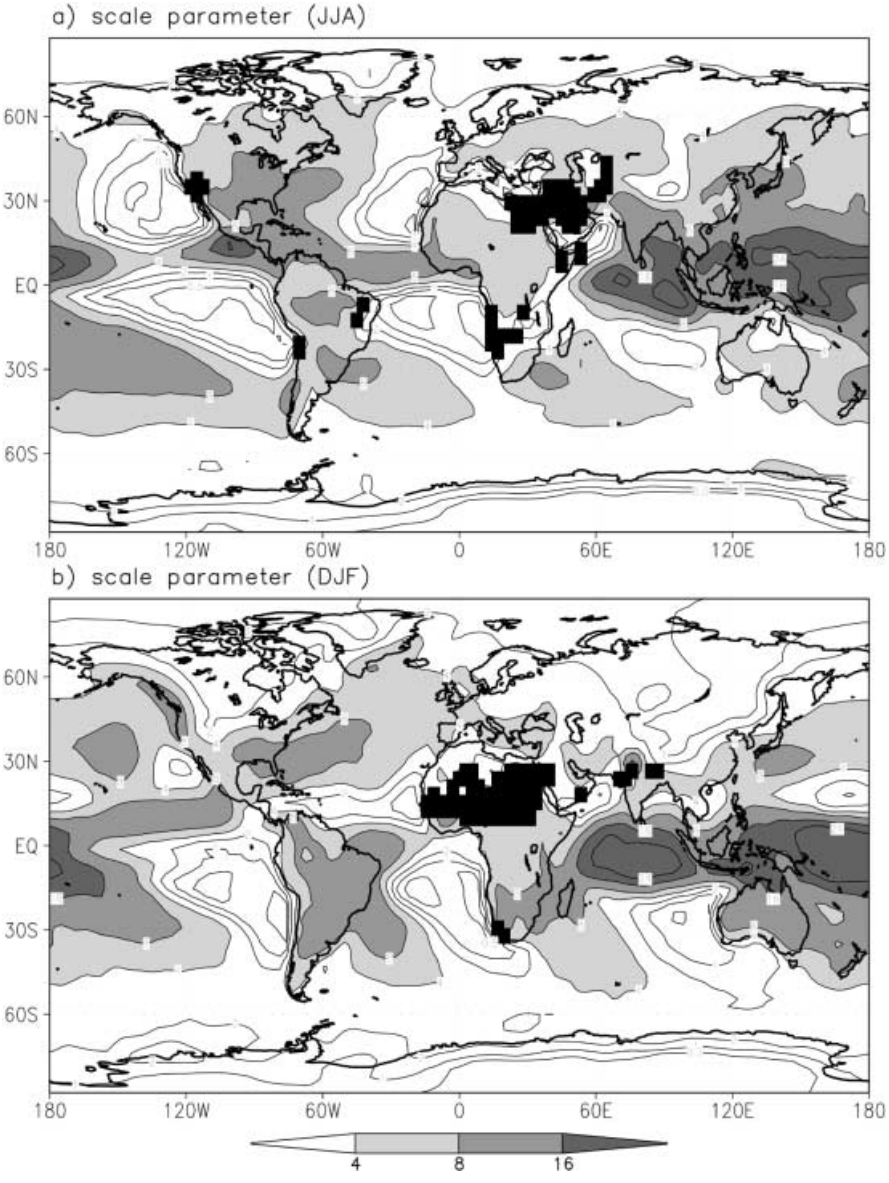

Fig. 8. Scale parameter (mm/day) for **a** JJA and **b** DJF, reference climate. Values greater than 4 are *shaded*, contours are at 0.5, 1, 2, 4, 8, 16, 24

Table 2. Mean values of simulated precipitation ($\bar{p}$), mean precipitation intensity (p_I), wet day probability (P_w), shape (α) and scale (β) parameters for JJA and DJF of the reference climate

	$\bar{p}$ [mm/d]	p_I [mm/d]	P_w	α	β [mm/d]
JJA					
land	2.24	3.81	0.47	0.82	5.28
ocean	3.18	3.87	0.78	0.78	6.18
DJF					
land	2.04	3.34	0.50	0.77	4.91
ocean	3.07	3.77	0.77	0.72	6.37

Wet day probability exhibits significant negative trends in most of the Southern Hemisphere continental areas. Particularly strong negative trends are found in the central and eastern parts of South America during JJA (exceeding 60%), western Australia and northern Africa during DJF.

6.4 Shape and scale parameters

Twenty first century relative trends in the shape and scale parameters of the gamma distribution for JJA and DJF are shown in Figs. 10 and 11, respectively. There is a negative trend in JJA shape parameter for the Northern Hemisphere land areas north to 45°N. The positive trend in southern Europe for JJA has a local maximum exceeding 20%. A similar maximum is observed over the eastern United States. During DJF the area of positive trend over continents spreads to larger regions of the mid- and high-latitudes of Eurasia, North America and eastern part of Australia. In general it can be noted that the magnitude of the trend in shape parameters over land is usually not exceeding 30% in few local maxima and 10% in zonal means.

The trend in the scale parameter for JJA (Fig. 11a) is generally positive over all land areas. The magnitude

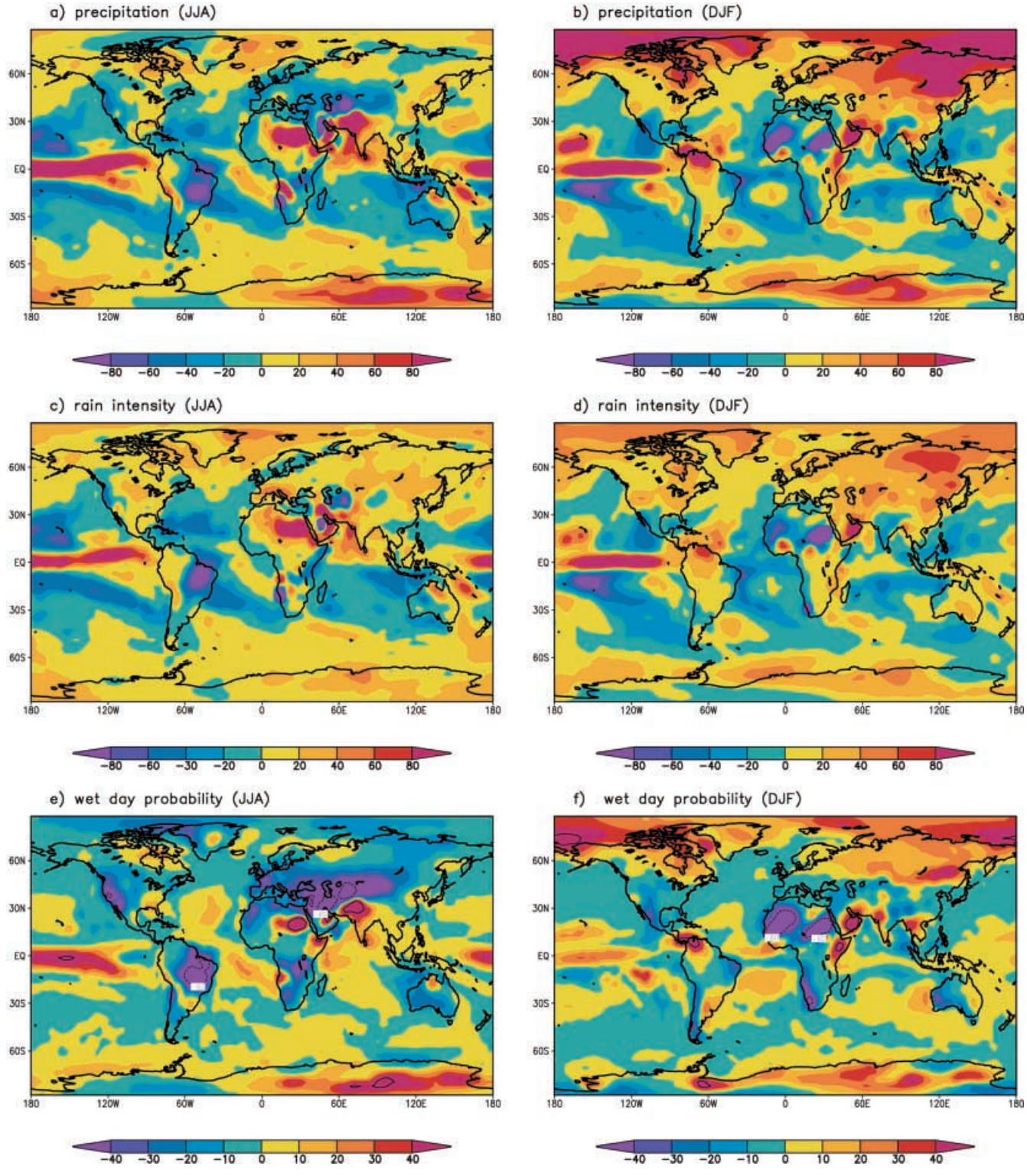

Fig. 9. Relative trends in mean JJA (*left column*) and DJF (*right column*) precipitation (*upper panels*), precipitaion intensity (*middle panels*) and wet day probability (*bottom panels*) simulated for 2000–2099, %/100 years

of the scale parameter trend is much higher than for the shape parameter. There is an area of maximum trend values (exceeding 60%) in Western Europe. Another maximum (reaching 50%) can be seen in the eastern part of Eurasia with a centre east of Lake Baikal.

During DJF (Fig. 11b) the strongest increase (reaching 80%) is found over northeastern Eurasia and

southern Siberia. Over the ocean a significant increase is observed in the Northern Hemisphere storm track regions and in the eastern equatorial Pacific. As in the case of the mean pattern for the reference climate, the distribution of the trends in scale parameter and precipitation intensity are very similar. The global pattern correlation is 0.83 (for JJA and DJF).

The secular trends for the these characteristics for JJA, DJF and annual means averaged over land, ocean areas and over the globe are summarized in Table 3. As a general feature one can see that the trends over oceans are usually an order less than those over land for all parameters. The scale parameter over land for all seasons undergoes the most rapid increase among other characteristics (about 20% for the century) accompanied by a decrease of the shape parameter (about –5%). The largest seasonal differences for the mean precipitation trends over land are mostly due to the strong precipitation increase in the northern high-latitudes during DJF and resulted in a 2.5 times larger relative trend for DJF (12.2%) in comparison to the JJA value (4.8%). Despite this difference the changes in precipitation intensity are of the same order (12.1% and 9.9% for DJF and JJA, respectively), which is related to the reduction of the wet day probability (over land) during JJA and a minor increase during DJF (–6.3% and 2.0%).

There is a significant similarity in the scale and reverse shape parameter trend patterns (the pattern correlation is about –0.5). It should be noted that this feature may represent an artifact due to a strong negative correlation between parameter estimators for the gamma distribution (Johnson and Kotz 1970).

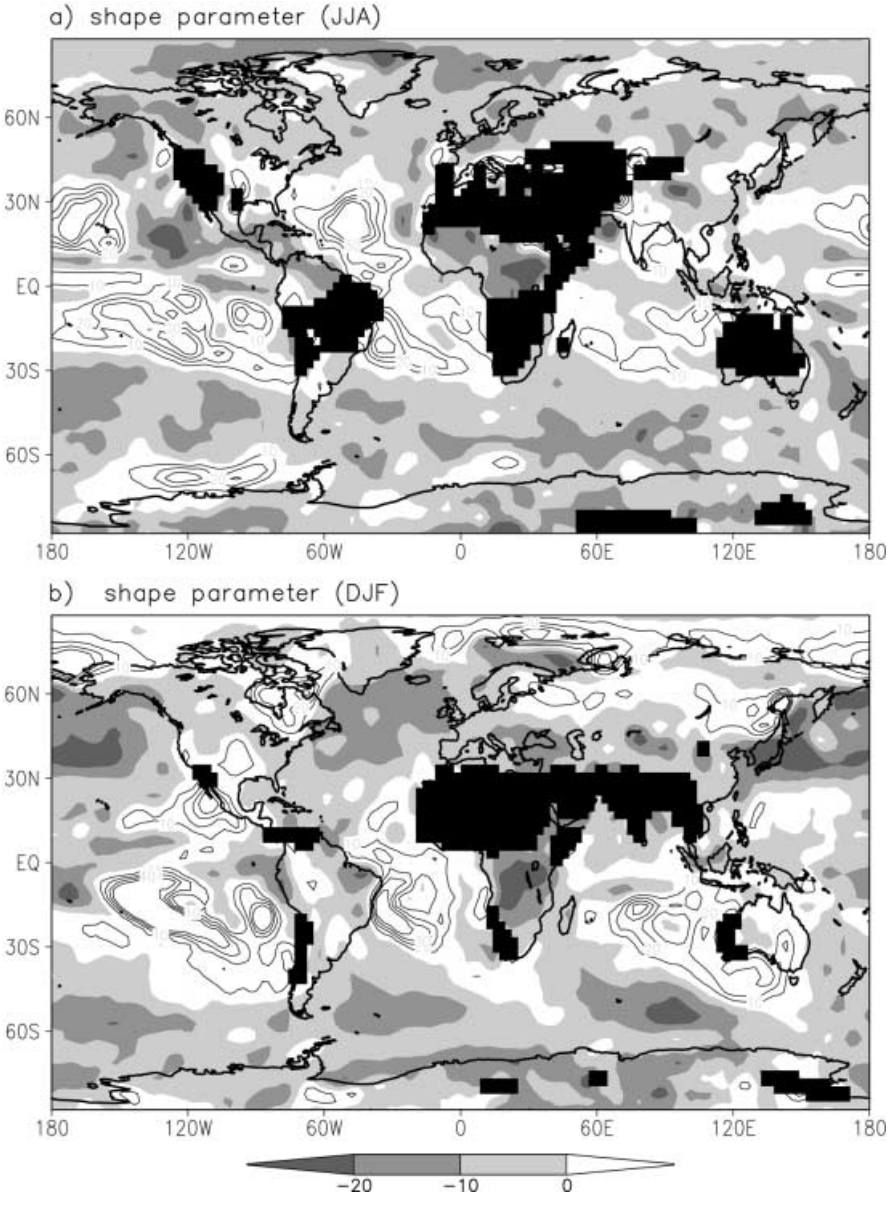

Fig. 10. Relative trend in shape parameter of the gamma distribution, **a** JJA and **b** DJF, 2000–2099, %/100 years; negative values are *shaded*, contours are at 10, 20, 30, 40

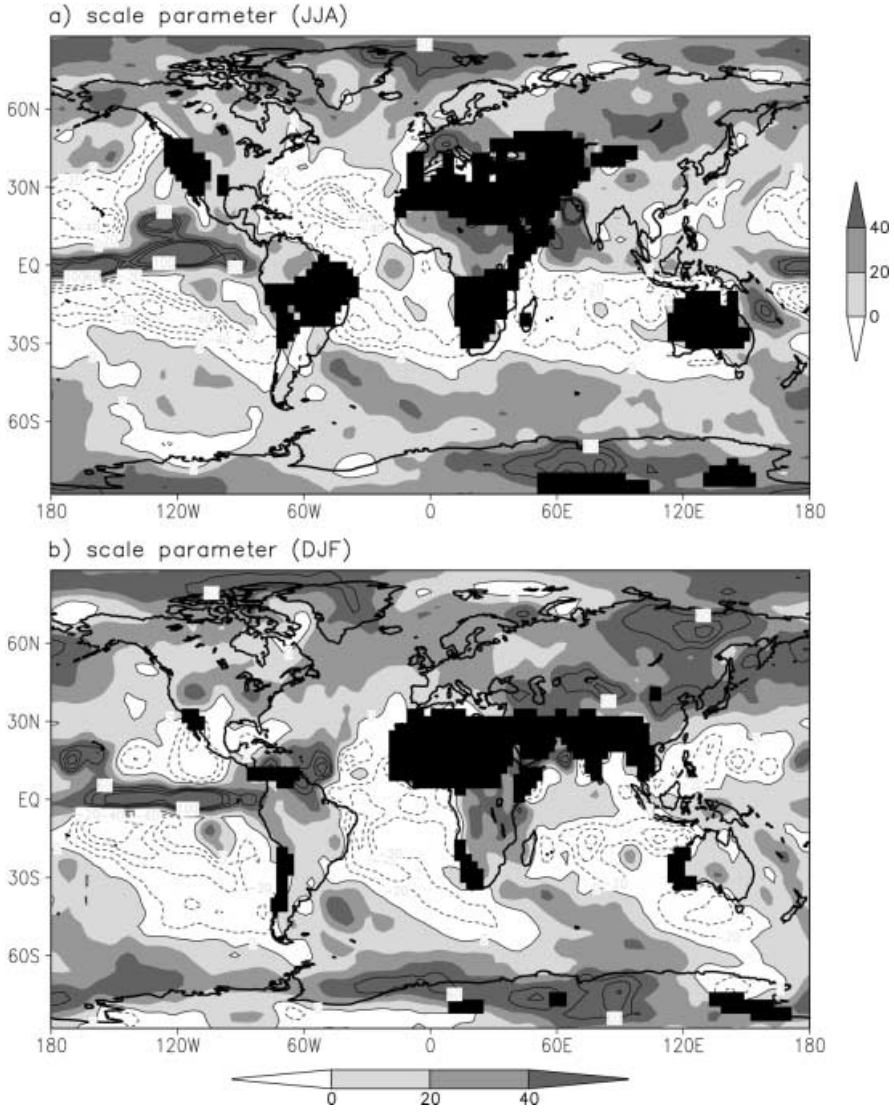

Fig. 11. Relative trend in scale parameter of the gamma distribution, **a** JJA and **b** DJF, 2000–2099, %/100 years; positive values are *shaded*, contours are at –80, –60, –40, –20, 0, 60, 80, 100

Table 3. 21st century absolute trends of precipitation characteristics. Trends are shown for annual means, JJA and DJF for the globe, land and ocean areas. In the parentheses the relative values (in %/100 years to the reference climate) are presented. Units for ($\bar{p}$), p_I and β trends are mm/day per century; for α and P_w trends – frac./100 yrs

		$\bar{p}$	p_I	P_w	α	β
JJA	land	0.108 (4.8)	0.376 (9.9)	–0.029 (–6.3)	–0.044 (–5.4)	1.032 (19.5)
	ocean	0.015 (0.5)	–0.035 (–0.9)	0.005 (0.6)	0.001 (0.2)	0.063 (1.0)
	globe	0.041 (1.4)	0.082 (2.1)	–0.005 (–0.8)	–0.009 (–1.1)	0.284 (4.8)
DJF	land	0.249 (12.2)	0.405 (12.1)	0.009 (2.0)	–0.029 (–3.9)	0.979 (20.0)
	ocean	–0.020 (–0.7)	–0.068 (–1.8)	0.007 (0.9)	0.001 (0.1)	0.033 (0.5)
	globe	0.057 (2.0)	0.067 (1.8)	0.008 (1.1)	–0.007 (–0.9)	0.261 (4.4)
Ann.	land	0.178 (8.2)	0.543 (12.8)	–0.014 (–2.8)		
	ocean	–0.003 (–0.1)	–0.053 (–1.3)	0.007 (0.9)		
	globe	0.049 (1.7)	0.117 (2.9)	0.001 (0.2)		

6.5 Heavy precipitation index

The secular trend in the contribution of the upper 10% quantile of the daily precipitation to the annual total (the index which was examined in the Sect. 3 for the United States during the twentieth century) is presented in Fig. 12. A significant positive trend is observed over all continental areas (except for Western Australia). Strongest trends are found in Africa with absolute maximum in its northern part and over the Arabian peninsula. Local maxima are also found in Europe (centered around the Alps), United States (south of the Great Lakes) and Mexico. These changes imply an increased probability of heavy rains (snowfalls) at the expense of light and moderate precipitation events.

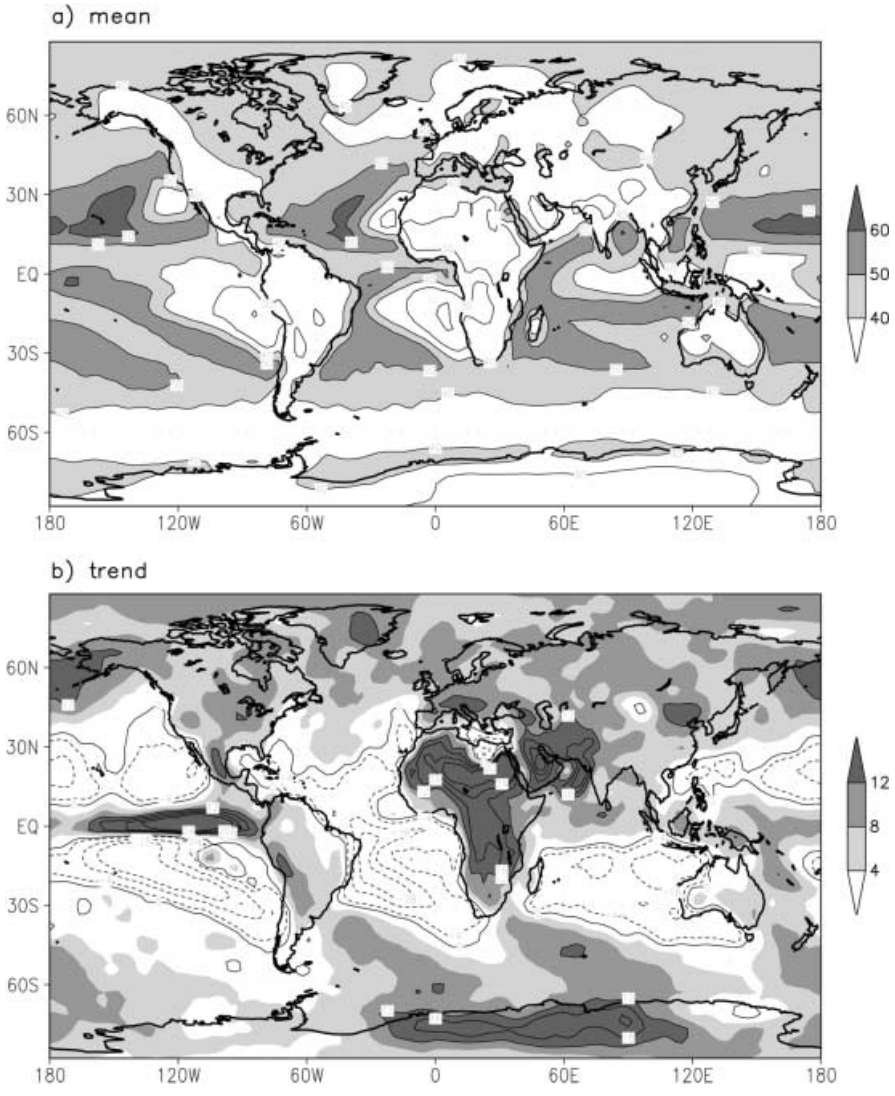

Fig. 12. Contribution of the upper 10% quantile of daily precipitation to the total precipitation, in %: **a** mean for the reference climate, values greater than 40 are *shaded*, contours are at 20, 30, 40, 50, 60; **b** trend for 2000–2099, %/100 years, values greater than 4 are *shaded*, contours are at –28, –16, –4, 0, 12, 16, 20, 24

7 Some regional examples

To illustrate long-term variations of the precipitation characteristics two 10° × 10° latitude/longitude densely inhabited areas were chosen in Central Europe (45°N–55°N, 5°E–15°E) and in the eastern United States (35°N–45°N, 75°W–85°W). Area averaged annual mean precipitation characteristics (mean precipitation, precipitation intensity, number of wet days, number of days with precipitation exceeding 90% quantile, 90% quantile-to-total precipitation ratio (see Fig. 12) and vertically integrated relative humidity) for 1900–2099 are presented in Fig. 13.

7.1 Europe

As can be seen from Fig. 13a, the mean precipitation for Central Europe is characterized by intense interdecadal variations. The highest values of the mean precipitation reached in the twenty first century since 2050 are comparable with the maxima of the decadal variations in the twentieth century. In general interdecadal variations dominate the long-term trends, although there is a positive trend for the twenty first century alone due to the minima in interdecadal variations in the first half of the century.

In contrast to the mean precipitation, the precipitation intensity (Fig. 13b) shows a rapid increase after 2030. This is related to the corresponding changes of the number of the wet days, Fig. 13c. This number steadily decreases from about 300 days per year (1940s) down to 255 at the end of the twenty first century. At the same time the number of days with precipitation exceeding 90% quantile (derived for the reference 1961–1990 climate) increased by about seven days in the twenty first century (Fig. 13d) with insignificant changes in the twentieth century. This is also reflected by the increased contribution of the heavy precipitation to the total annual precipitation amount (the index discussed in Sect. 3), which increased from 40% to 50% during 2000–2099 (Fig. 13e).

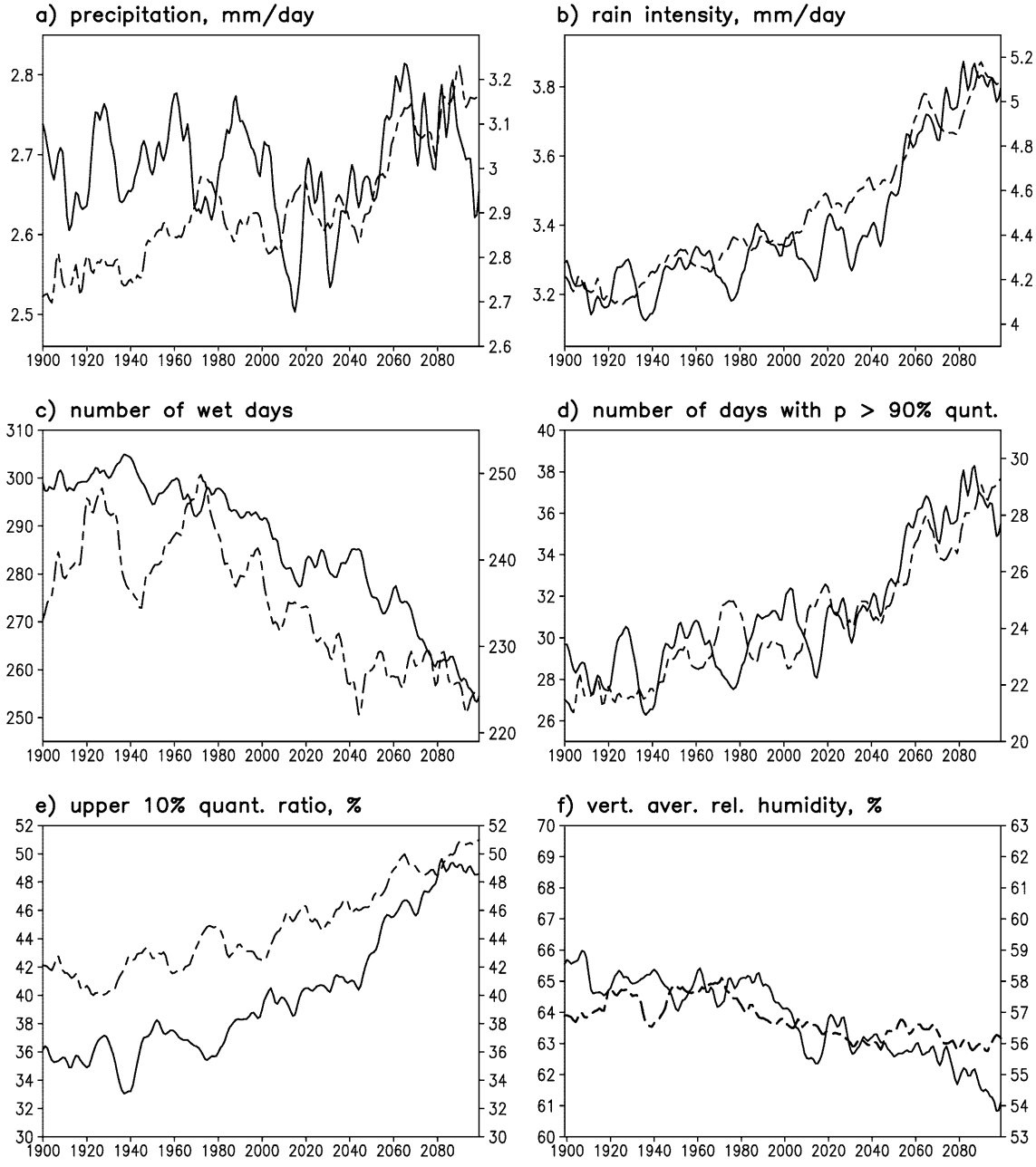

Fig. 13. Precipitation characteristics for the central Europe (*solid lines*) and eastern United States (*dashed lines*), 10 year running means. *Y-axis labels* are on the *left side* of the plots for the Europe and on the *right side* for the US

In Fig. 13f the vertically integrated relative humidity through the free troposphere (850–300 hPa) is presented. A slight negative trend is observed starting from the end of the twentieth century. The correlation between this quantity and the number of wet days (Fig. 13c) is 0.84. The small changes of the relative humidity are negligible for the increasing moisture content as the corresponding increase of the saturation specific humidity is about 35–40% due to the 4–5 K annual mean temperature growth in the low troposphere at the end of the simulation. On the other hand, these changes are strong enough to affect the probability of precipitation occurrence.

7.2 United States

For the eastern United States the long-term changes of the mean precipitation (Fig. 13a) in the twenty first century are dominant over interdecadal variations. A rapid precipitation increase is observed since the middle of the twenty first century, preceded by a relatively sta-

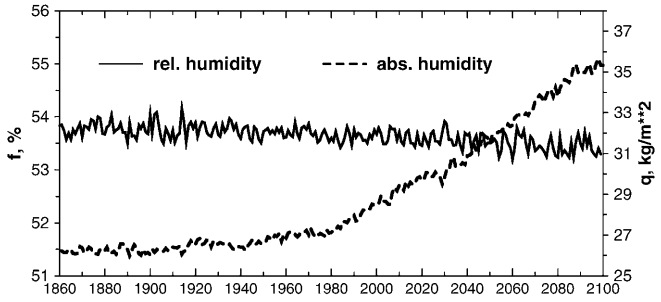

Fig. 14. Annual mean global values of relative humidity f (in %) vertically averaged for 850–300 hPa and vertically integrated absolute humidity q (in kg/m^2). Averaging for land and ocean separately produces the same tendencies

ble period. The interdecadal variability of the precipitation intensity is much weaker, and a clear positive trend can be seen starting from the second third of the twentieth century (Fig. 13b).

As in the case for Central Europe, the number of wet days significantly decreased in the twenty first century (Fig. 13c), while the twentieth century is characterized by interdecadal variations with an amplitude of about 15 days. Again the number of days with heavy precipitation was steadily increasing during 1900–2099 (Fig. 13d) with an enhanced rate in the twenty first century (about six days).

The heavy precipitation index and vertically integrated relative humidity are shown on Fig. 13e, f. As for Europe the vertically integrated relative humidity is highly correlated (0.71) with the number of wet days.

8 Discussion

The increase of the greenhouse gas concentrations in the transient climate change experiment with the ECHAM4/OPYC3 AOGCM predicts considerable changes in the mean characteristics of the global hydrological cycle during the twenty first century. These changes were accompanied by a significant modification of the daily precipitation probability distribution. A simple statistical model based on the gamma distribution has showed a reliable fit to the simulated daily precipitation probabilities for most of the land areas.

Changes in the daily precipitation over land can be characterized by, in general, a slight decrease of the shape parameter that means increasing skewness of the probability distribution (for all seasons except winter when positive shape parameter trends were found in northern high-latitudes and large areas in the Southern Hemisphere). The scale parameter changes over land are positive with rare exceptions for all seasons. An increase of the scale parameter means a stretching of the distribution with exponential increase of the heavy precipitation events. The relative changes of the scale parameter are usually several times stronger than the changes of the shape parameter. The fact that the gamma distribution changes caused by increased total precipitation are reflected mostly by a corresponding rescaling of the distribution with relatively small changes in its shape was found by analysis of the observed data by Groisman et al. (1999). However, as was found in our study, the shape of the distribution may also experience significant transformations in some regions which should be taken into account when estimating scenarios of precipitation distribution changes. This is the case, in particular, with significant positive trends reaching 20% (0.15–0.2 increase of the shape parameter) in the central United States (for both JJA and DJF) and southern Europe during JJA. The increase of the shape parameter in southern Europe was accompanied by the strongest increase (more that 60%) of the scale parameter.

A clear reduction in the probability of a wet day was observed, in particular, for the large areas in the northern mid-latitudes and subtropics. Despite this decrease the relative contribution of heavy precipitation has grown (Fig. 12) due to the corresponding increase of the scale parameter of the gamma distribution (and precipitation intensity respectively). This implies a more extreme climate with higher probabilities of droughts and heavy precipitation events.

Based on the observation that the global averaged relative humidity is broadly conserved within a range of climate forcing, an increased warming will imply an increase of total moisture in the atmosphere in accordance with Clausius-Clapeyron equation. This is illustrated by Fig. 14. Does the conservation of the relative humidity reflect fundamental properties of the atmosphere's physics and what is the range of external forcing for this conservation to hold? Or is it a result of simplified GCM parameterizations of precipitation and cloud formation which usually fix relative humidity profile? These questions require a closer consideration.

Another important question is a rescaling of the GCM results in order to obtain daily precipitation statistics and their change locally. This is of major importance for the extreme precipitation properties since the upper tail of the precipitation distribution suffers most from coarse resolution representation in the GCMs. One well-known approach is the use of empirically based downscaling techniques. The disadvantage of these methods is the requirement of sufficiently long observed data for the considered location to train a downscaling model. Another way is to use more common knowledge such as the spatial correlation of the precipitation process and a relation between point and area averaged variations of daily precipitation (Osborn and Hulme 1997). A successful use of the gamma distribution with the model daily precipitation may help to construct a statistical downscaling model assuming precipitation to be identically distributed on different spatial scales and taking into account scaling properties of the rainfall processes.

Acknowledgements We thank T. Karl and R. Knight for their kind permission to reproduce Fig. 2 from (Karl and Knight 1998).

We also thank R. Voss, I.I.Mokhov, A.V.Eliseev and anonymous reviewer for helpful comments on the text.

References

Arpe K, Roeckner E (1999) Simulation of the hydrological cycle over Europe: model validation and impacts of increasing greenhouse gases. Adv Water Resour 23: 105–119

Arpe K, Bengtsson L, Golitsyn GS, Mokhov II, Semenov VA, Sporyshev PV (1999) Analysis and modeling of the hydrological regime variations in the Caspian Sea basin. Dokl Earth Sci 366: 552–556

Bradley RS, Diaz HF, Eischeid JK, Jones PD, Kelly PM, Goodess CM (1987) Precipitation fluctuation over Northern Hemisphere land areas since mid-19th century. Science 237: 171–175

D'Agostino RB, Stephens MA (1986) Goodness-of-fit techniques. Marcel Dekker, New York, pp 560

Dai A, Fung IY, DelGenio AD (1997) Surface observed global land precipitation variations during 1900–88. J Clim 10: 2943–2962

Diaz HF, Bradley RS, Eischeid JK (1989) Precipitation fluctuation over global land areas since the late 1800s. J Geophys Res 94: 1195–1210

Gregory JM, Mitchell JFB (1995) Simulation of daily variability of surface temperature and precipitation over Europe in the current and 2 $\times CO_2$ climates using the UKMO climate model. Q J R Meteorol Soc 121: 1451–1476

Gregory JM, Wigley TML, Jones PD (1993) Application of Markov models to area-average daily precipitation series and interannual variability in seasonal totals. Clim Dyn 8: 299–310

Groisman PY, Easterling DR (1994) Variability and trends of total precipitation and snowfall over the United States and Canada. J Clim 7: 184–205

Groisman PY, Karl TR, Easterling DR, Knight RW, Jamason PF, Hennessy KJ, Suppiah R, Page CM, Wibig J, Fortuniak K, Razuvaev VN, Douglas A, Førland E, Zhai PM (1999) Changes in the probability of heavy precipitation: important indicators of climatic change. Clim Change 42: 243–283

Gruza G, Rankova E, Razuvaev V, Bulygina O (1999) Indicators of climate change for the Russian Federation. Clim Change 42: 219–242

Hennessy KJ, Gregory JM, Mitchell JFB (1997) Changes in daily precipitation under enhanced greenhouse conditions. Clim Dyn 13: 667–680

Hoskins JRM (1990) L-moments: analysis and estimation of distributions using linear combinations of order statistics. J R Statist Soc B 52: 105–124

Houghton JT, Callander BA, Varney SK (eds) (1992) Climate change 1992: the supplementary report to the IPCC scientific assessment. Cambridge University Press, Cambridge, UK, pp 198

Houghton JT, Miera Filho LG, Callander BA, Harris N, Kattenberg A, Maskell K, (eds) (1996) Climate change 1995: the science of climate change. Cambridge University Press, Cambridge, UK, pp 572

Hu ZZ, Bengtsson L, Arpe K (2000) Impact of global warming on the Asian winter monsoon in a coupled GCM. J Geophys Res 105: 4607–4624

Johnson NL, Kotz S (1970) Distributions in statistics: continuous univariate distributions–1. Houghton Mifflin, Boston, USA

Juras J (1994) Some common features of probability distribution for precipitation. Theor Appl Climatol 49: 69–76

Karl TR, Knight RW (1998) Secular trends of precipitation amount, frequency, and intensity in the United States. Bull Am Meteorol Soc 79: 231–241

Karl TR, Knight RW, Easterling DR, Quayle RG (1996) Indices of climate change for the United States. Bull Am Meteorol Soc 77: 279–292

Katz RW (1977) Precipitation as a chain-dependent process. J Appl Meteorol 16: 671–676

Katz RW (1999) Extreme value theory for precipitation: sensitivity analysis for climate change. Adv Water Resour 23: 133–139

Kharin VV, Zwiers FW (2000) Changes in the extremes in an ensemble of transient climate simulations with a coupled atmosphere–ocean GCM. J Clim 13: 3760–3788

McGuffie K, Henderson-Sellers A, Holbrook N, Kothavala Z, Balachova O, Hoekstra J (1999) Assessing simulation of daily temperature and precipitation variability with global climate models for present and enhanced greenhouse climates. Int J Climatol 19: 1–26

New M, Hulme M, Jones P (1999) Representing twentieth-century space-time climate variability. Part I: development of a 1961–90 mean monthly terrestrial climatology. J Clim 12: 829–856

New M, Hulme M, Jones P (2000) Representing twentieth-century space-time climate variability. Part II: development of 1901–96 monthly grids of terrestrial surface climate J Clim 13: 2217–2238

Oberhuber JM (1993) Simulation of the Atlantic circulation with a coupled sea ice – mixed layer – isopycnal general circulation model. Part I: model description. J Phys Oceanogr 23: 808–829

Osborn TJ, Hulme M (1997) Development of a relationship between station and grid-box rainday frequencies for climate model evaluation. J Clim 10: 1885–1908

Roeckner E, Arpe K, Bengtsson L, Christoph M, Claussen M, Dümenil L, Esch M, Giorgetta M, Schlese U, Schulzweida U (1996a) The atmospheric general circulation model ECHAM-4: model description and simulation of present-day climate. Rep 218, Max-Planck-Institut für Meteorologie, Hamburg, Germany, pp 90

Roeckner E, Oberhuber JM, Bacher A, Christoph M, Kircher I (1996b) ENSO variability and atmospheric response in a global coupled atmosphere–ocean GCM. Clim Dyn 12: 737–754

Roeckner E, Bengtsson L, Feichter J, Lelieveld J, Rohde H (1999) Transient climate change simulations with a coupled atmosphere–ocean GCM including the tropospheric sulfur cycle. J Clim 12: 3004–3032

Stendel M, Roeckner E (1998) Impacts of horizontal resolution on simulated climate statistics in ECHAM4. Rep 253, Max-Planck-Institut für Meteorologie, Hamburg, Germany, pp 57

Stern RD, Coe R (1984) A model fitting analysis of daily rainfall data. J R Stat Soc A 147: 1–34

Suppiah R, Hennessy KJ (1998) Trends in total rainfall, heavy rain events and number of dry days in Australia, 1910–1990. Int J Climatol 10: 1141–1164

Thom HCS (1958) A note on the gamma distribution. Mon Weather Rev 86: 117–121

Trenberth KE (1998) Atmospheric moisture residence times and cycling: implications for rainfall rates and climate change. Clim Change 39: 667–694

Ulbrich U, Christoph M (1999) A shift of the NAO and increasing storm track avtivity over Europe due to anthropogenic greenhouse gas forcing. Clim Dyn 15: 551–559

Vinnikov KY, Groisman PY, Lugina KM (1990) Empirical data on contemporary global climate changes (temperature and precipitation). J Clim 3: 662–677

Voss R, May W, Roeckner E (2002) Enhanced resolution modelling study on anthropogenic climate change: changes in extremes of the hydrological cycle. Int J Climatol (in print)

Wang XLL, Cho HR (1997) Spacial-temporal structures of trend and oscillatory variabilities of precipitation over Northern Eurasia. J Clim 10: 2285–2298

Wilks DS (1990) Maximum likelihood estimation for the gamma distribution using data containing zeros. J Clim 3: 1495–1501

Wilks DS (1995) Statistical methods in atmospheric science. Acedemic Press, New York, pp 467

Woolhiser DA, Roldan J (1982) Stochastic daily precipitation models. Part 2: comparison of the distribution of amounts. Water Resour Res 18: 1461–1468

Xie PP, Arkin PA (1997) Global precipitation: A 17-year monthly analysis based on gauge observations, satellite estimates, and numerical model outputs. Bull Am Meteorol Soc 78: 2539–2558

Zhai PM, Sun AJ, Ren FM, Liu XN, Gao B, Zhang Q (1999) Changes of climate extremes in China. Clim Change 42: 203–218

Zwiers FW, Kharin VV (1998) Changes in the extremes of the climate simulated by CCC GCM2 under CO_2 doubling. J Clim 11: 2200–2222